Korean J. Chem. Eng., **30**(10), 1843-1854 (2013)
DOI: 10.1007/s11814-013-0154-0

Mixing of initially stratified miscible fluids in an eccentric stirred tank: Detached eddy simulation and volume of fluid study

Feng Ling Yang*,,†, Shen Jie Zhou*,**, Cui Xun Zhang***, and Gui Chao Wang***

*School of Mechanical Engineering, Shandong University, Jinan 250061, China
**Key Laboratory of High Efficiency and Clean Mechanical Manufacture, Shandong University, Ministry of Education, Jinan 250061, China
***Tianli Drying Equipment Incorporated Company, Shandong Province Academy of Sciences, Jinan 250014, China
(*Received 15 June 2013 • accepted 11 August 2013*)

Abstract−Mixing of two stratified miscible fluids in an eccentric stirred tank agitated by a four pitched-blade turbine was studied by using the detached eddy simulation (DES) model and volume of fluid (VOF) method. The fluids were operated in the transitional and mildly turbulent flow regimes. Interfaces between the two miscible fluids during the mixing processes were captured and mixing times were computed. Effects of the Richardson number and eccentricity on the mixing times were quantificationally analyzed. Results show that the spatial and temporal variations of volume fractions of the fluids can be well captured by the method presented in this study. Mixing time increases with the increase of Richardson number. Effect of eccentricity on mixing time depends on Richardson number and the eccentric agitation scheme is not advisable to use to blend the low-viscosity miscible fluids starting from a stratified state, especially for lower Richardson values.

Key words: Stirred Tank, Stratification, Miscible Fluids, Mixing, Detached Eddy Simulation (DES), Volume of Fluid (VOF)

INTRODUCTION

Mixing of fluids with different viscosities and densities is a basic unit operation in food processing, (petro) chemical, fermentation, pharmaceutical, polymerization and other process industries. Viscosity and density differences between the fluids will inevitably affect the flow patterns and, therefore, the homogenization process. To date, mixing of immiscible fluids in baffled stirred tanks, which involves the mixing of a dispersed fluid phase in a continuous fluid phase, has received much consideration [1-7]. However, less attention has been devoted to the mixing of miscible fluids. Among the relevant studies, the objective is mainly to take two or more miscible fluids and blend them to a predetermined degree of homogeneity [8]. The time taken to reach this degree of homogeneity and to get a uniform mixture of miscible liquids is called mixing time, which has been investigated extensively.

Some of the studies on the mixing of miscible liquids in stirred tanks are presented as follows. Smith and Schoenmakers [9] investigated the assimilation of various aqueous solutions into water in a stirred vessel. The mixing times were measured using the conductivity method. It was found that, when blending small quantities of high viscosity fluid into a turbulently stirred low viscosity bulk, the viscosity of the additives had little effect on the mixing time except when discrete masses came in contact and adhered to solid surfaces within the mixing vessel. It was the density difference that caused longer mixing time. The effect of density difference on the mixing of two miscible fluids in a semi-batch reactor was studied by Bouwmans and van den Akker [10]. It was identified that density differences are more likely to delay the mixing process than viscosity differences. Bouwmans et al. [11] visualized the turbulent mixing of small additions of liquid, which has a density lower than that of the bulk. They also found that the effects of density differences on mixing times are stronger than that of viscosity differences. In addition, they defined the Richardson number (Ri), which includes the density difference between the liquids to be mixed. Gogate and Pandit [12] studied the mixing of tracer fluid and the bulk in a stirred tank. The mixing time was found to be proportional to the density difference. Mann et al. [13] considered the unsteady semi-batch mixing of miscible fluids in a plant-scale stirred tank by using electrical resistance tomography (ERT). The experiments involved injecting a small quantity of brine solution into water and reconstructing the resistivity field from the sensors installed in the tank. Through this method, the laminar mixing patterns were clearly illustrated. The ERT method was also employed by Kim et al. [14] to measure the mixing of two miscible liquids with distinct conductivities in a tank agitated by a Rushton turbine impeller. The mixing process was visualized, the mixing times and the dispersion velocity of the secondary liquid in the primary liquid were determined. Madras and McCoy [15] simulated the diffusion of tracer into a miscible bulk fluid by the population balance modelling (PBM) approach. The interfacial area between dispersed and bulk fluids, which controls the transfer of a scalar molecular property, was successfully modelled. Direct numerical simulation (DNS) on the turbulent mixing of miscible fluids with different densities and the same viscosities was conducted by Jang and de Bruyn Kops [16]. It was observed that density ratio has little effect on the mean energetics of isotropic homogeneous turbulence.

In addition to the mixing operations involving the addition of a small amount of the liquid with a difference in the viscosity and/or density into a bulk of another liquid, mixing of miscible liquids ini-

†To whom correspondence should be addressed.
E-mail: fly@sdu.edu.cn

tially segregated and stably stratified systems has also been studied. For example, van de Vusse [17] discussed the mixing of miscible liquids starting from stable stratifications in batch operation. An optical technique, known as the Schlieren method, was used to determine the mixing time. In the turbulent flow regime, mixing time was found to be equal to the ratio of the liquid volume to the pumping capacity of the impeller. Rielly and Pandit [18] examined the mixing of two layers with different viscosities, initially stratified as a result of a density difference in a batch mixing situation. The authors found that mixing time is a function of Richardson number. Recently, homogenization of miscible liquids with different densities and the same kinematic viscosity in a stirred tank starting from a stratified state was numerically studied by Derksen [19] using the lattice-Boltzmann method (LBM). The influence of Richardson number on the flow field and the density distribution was examined. Subsequently, Derksen [20] modeled the effect of density and viscosity differences on the mixing times. The fluids were operated in transitional and mildly turbulent regimes. The author concluded that mixing times increase steeply with increasing Ri. The viscosity ratio has a much weaker influence on the mixing time. To the best of our knowledge, these are the first two papers that discuss the impact of density and viscosity differences as well as stratification on the mixing processes in stirred tanks. And most investigations on the mixing of stratified fluids have been given much attention in environmental fluid mechanics [21-25].

In this paper, we discuss the stratified mixing of two miscible fluids with different viscosity and density in an eccentric stirred tank. The unbaffled stirred tank was chosen for the purpose of validating the capability of eccentric agitation in the mixing of the miscible liquids, and the unbaffled concentrically stirred tank was chosen for the purpose of comparison. It has been identified that eccentric agitation performs better than concentric agitation as it enhances the axial circulation in the tank. This is done by employing eccentricity as a measure to trigger chaos. In the mixing of two miscible fluids, the mixing process is dominated by the properties of the two fluids. The stirred tank configurations used here are the same as those investigated by Yang et al. [26] when they simulated the mixing processes of introducing a scalar tracer into a miscible bulk fluid by detached eddy simulation (DES) model. In that case, the mixing process was determined mainly by the bulk fluid. In the present study, spatial and time evolutions of the interfaces between the two miscible fluids, which will be eliminated when a homogeneous mixing state is obtained, are simulated by using the volume of fluid (VOF) method, which can be used to study the mixing of immiscible and/or stably stratified miscible fluids.

The first application of VOF to the modeling of fluids flow in stirred tanks was reported about ten years ago by Serra et al. [27]. They simulated the flow with wavy free-surface in a fully baffled stirred tank. The numerical predictions were compared with the LDV measurements and some discrepancies were observed. Haque et al. [28] for the first time used a homogeneous multiphase flow model coupled with VOF to determine the gas-liquid interface in unbaffled vessels. The predicted liquid surface profiles using VOF are generally in good agreement with experimental measurements. Cartland Glover and Fitzpatrick [29] used the same approach for the modeling of vortex in an unbaffled stirred tank operating in the turbulent flow regime. A reasonable representation of the flow phenomena was achieved. However, some questions remain over the accuracy of the modeling technique. They suggested that the numerical model should include the whole domain. Besides, large eddy simulation, detached eddy simulation, scale adaptive simulation or Reynolds stress model that can improve the calculation of turbulence should be adopted. The same conclusion was also reached by Torré et al. [30] when they used the single-phase RANS model and multiphase inhomogeneous CFD approach for modeling the turbulent flow in partially baffled stirred tanks. The combination of RSM and VOF was first employed by Mahmud et al. [31] to simulate the turbulent flow with free-surface vortex in an unbaffled reactor agitated by a cylindrical magnetic stirrer. The predicted general shapes of the liquid free-surface are in good agreement with the experimental measurements, but the vortex depth was underpredicted. In a recent study, a two-phase, turbulent and transient flow in an unbaffled stirred tank was modeled by Lamarque et al. [32] using the LES model and front-tracking method. Evolution of free-surface vortex height with time during its growth was successfully captured. Very recently, VOF together with the LES model was used to predict the free liquid surface motion in a stirred tank by Jahoda et al. [33]. The predicted results of the free surface elevation/depression were in good agreement with the experimental investigations.

The flow dynamics and mixing efficiency of miscible fluids depend not only on the Reynolds number (Re), but also on the Richardson number, which is defined as the ratio of buoyancy forces to inertial forces. If Ri is much less than unity, buoyancy is unimportant in the flow. If it is much greater than unity, buoyancy is dominant in the sense that there is insufficient kinetic energy to homogenize the fluids. If Ri is on the order of unity, then the flow is likely to be buoyancy driven. Here we discuss three cases: Ri less than one, approximately equals to one, and slightly greater than one. In addition, the effect of eccentricity on the stratification mixing process was also considered.

The rest of this paper is organized as follows: Section 2 presents the stirred system and the operating conditions. In section 3, the governing equations, computational grid and numerical solution method are described. In section 4, the effect of Ri and eccentricity on the stratification is discussed and the mixing times are quantificationally analyzed. Finally, conclusions are summarized in section 5.

STIRRED SYSTEM

Configurations of the investigated stirred tank and impeller are given in Fig. 1. The system is an unbaffled, flat-bottomed, cylindrical tank (of diameter T=0.15 m) agitated by a down-pumping pitched-blade turbine with four blades (named as PBT-4), each angled at 30° to the horizontal and is attached to a hub mounted on the impeller shaft with a diameter d=0.008 m. The top of the stirred tank is covered with a lid to inhibit vortex formation and air entrainment. The thickness and width of the impeller blade are t_b=0.001 m and w_b=0.01 m, respectively. The tank is filled with two miscible fluids: glycerin (volume fraction: 50%) and water at 20 °C. The total height of the fluids is H=T. The lighter liquid, water, occupies the upper part of the tank, and the heavier liquid, glycerin, is located in the lower part. The interface is at half the tank height: z=0.5H. In the numerical simulations, the fluids are assumed to be incompressible. The density and dynamic viscosity of water is ρ_w=998 kg·m^{-3} and μ_w=1×

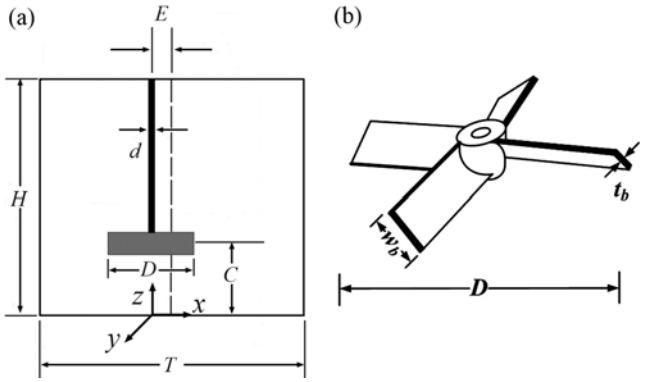

Fig. 1. Configuration of the unbaffled stirred tank (a) with a pitched blade impeller (b).

10^{-3} Pa·s. For glycerin, the density is ρ_g=1126 kg·m^{-3} and the dynamic viscosity is μ_g=6×10^{-3} Pa·s.

In addition to the Richardson number, the effect of the impeller locations in the stirred tank on the evolution of the interface between the two miscible fluids during the mixing process was also taken into account. The concentric and eccentric agitations were investigated. As for the concentric agitation, the shaft of the impeller was concentric with the axis of the tank. For the eccentric agitation, the impeller was positioned at an off-axis location of E=0.015 m from the tank axis, which corresponds to an eccentricity of e=2E/T=0.2. In both cases, the diameter of the impeller is D=T/3 and the impeller off-bottom clearance is C=T/3. Reynolds and Richardson numbers considered here are defined as Re=(ρND^2/μ) and Ri=(g$\Delta\rho$/ρN^{2}D), respectively. In these two expressions, g is gravitational acceleration, ρ is the volume-averaged density of the fluids in the tank, and μ is the volume-averaged viscosity. Since the density difference between the two fluids studied here is not so large ($\Delta\rho/\rho\approx$0.12), the Ri number was altered by adjusting the impeller rotation speeds, which are N= 4, 5 and 10 s^{-1} (clockwise as viewed from the above). With the aforementioned settings, the Ri number is in the range of 0.236-1.478. The Reynolds number ranges about from 3000 to 7600, indicating that the mixing is operated in transitional and mildly turbulent flow regimes.

NUMERICAL SIMULATION

1. Flow Field Modeling

The fluid flow in the stirred tank was simulated by the DES model. Capability of this model in simulating the turbulent flow and mixing processes in stirred tanks has been validated by several authors [26,34,35] very recently. The DES model is formulated by replacing the distance function d in the Spalart-Allmaras (S-A) model with a modified distance function:

$$\tilde{d}=\min\{d;C_{DES}\Delta\} \tag{1}$$

where C_{DES}=0.65 is the model empirical constant and Δ is the largest dimension of the grid cell in question. This modification of the S-A model changes the interpretation of the model substantially. In regions close to the wall, where d<$C_{DES}\Delta$, it behaves as a RANS model. Away from the wall, where d>$C_{DES}\Delta$, it behaves in a Smagorinsky-like manner and is changed to the LES model. The governing equation of DES model can be given as follows:

$$\frac{\partial\tilde{\nu}}{\partial t}+\langle u_i\rangle\frac{\partial\tilde{\nu}}{\partial x_i}=C_{b1}(1-f_{t2})\tilde{S}\tilde{\nu}+\frac{1}{\sigma}\left\{\frac{\partial}{\partial x_i}\left[(\nu+\tilde{\nu})\frac{\partial\tilde{\nu}}{\partial x_i}\right]+C_{b2}\left(\frac{\partial\tilde{\nu}}{\partial x_i}\right)^2\right\}-\left(C_{w1}f_w-\frac{C_{b1}}{c^2}f_{t2}\right)\left(\frac{\tilde{\nu}}{d}\right)^2 \tag{2}$$

where u_i is velocity, $\tilde{S}$ is modified vorticity, ν is molecular viscosity, $\tilde{\nu}$ is modified turbulent viscosity that linked to the turbulent viscosity ν_t and a wall function f_{v1} by

$$\tilde{\nu}=\nu_t/f_{v1},\quad f_{v1}=\frac{\chi^3}{\chi^3+C_{v1}^3},\quad \chi=\frac{\tilde{\nu}}{\nu} \tag{3}$$

The modified vorticity $\tilde{S}$ is defined in terms of the magnitude of vorticity S in the following equation:

$$\tilde{S}=S+\frac{\tilde{\nu}}{c^2d^2}f_{v2},\quad f_{v2}=1-\frac{\chi}{1+\chi f_{v1}},\quad f_{v3}=\frac{(1+\chi f_{v1})(1-f_{v2})}{\chi} \tag{4}$$

The functions f_{t2} and f_w in Eq. (2) are defined as:

$$f_{t2}=C_{t1}\exp(-C_{t2}\chi^2) \tag{5}$$

$$f_w=g\left(\frac{1+C_{w3}^6}{g^6+C_{w3}^6}\right),\quad g=r+C_{w2}(r^6-r),\quad r=\frac{\tilde{\nu}}{\tilde{S}c^2d^2} \tag{6}$$

DES model was proposed based on the one-equation S-A model. Since then, some variants, such as the DES model based on the SST k–ω and Realizable k–ε model, have been proposed by Strelets [36] and Li and Ren [37], respectively. No matter what kind of RANS model was used, the principle was the same. In this paper, the DES model proposed by Spalart et al. [38], which is referred to as the standard edition, is adopted. The closure coefficients in the governing equation of DES model are given as follows:

σ=2/3, c=0.41, C_{b1}=0.1335, C_{b2}=0.622, C_{w1}=C_{b1}/k^2+(1+C_{b2})/σ, C_{w2}=0.3, C_{w3}=2, C_{v1}=7.1, C_{t1}=1.1 and C_{t2}=2.

2. Simulation of the Interface

The interface between the two miscible fluids was captured by the VOF method, which is a surface-tracking technique applied to a fixed Eulerian mesh. In this method, the two fluids share the same velocity and turbulence fields within the whole domain, which can be determined by solving a single set of governing transport equations with the volume-weighted mixture density and viscosity. The mass and momentum conservation equations of the VOF model are given as follows:

$$\frac{\partial\rho}{\partial t}+\nabla\cdot(\rho\mathbf{u})=0 \tag{7}$$

$$\frac{\partial}{\partial t}(\rho\mathbf{u})+\nabla\cdot(\rho\mathbf{u}\mathbf{u})=-\nabla p+\nabla\cdot[\mu(\nabla\mathbf{u}+\nabla\mathbf{u}^T)]+\rho\mathbf{g}+\mathbf{F} \tag{8}$$

where t is time, **u** is velocity, p is pressure, **g** is gravitational acceleration, **F** is the force acting on the fluid element, ρ is the volume-averaged density of the fluids in the tank, μ is the volume-averaged viscosity:

$$\rho=\alpha_w\rho_w+\alpha_g\rho_g \tag{9}$$

$$\mu=\alpha_w\mu_w+\alpha_g\mu_g \tag{10}$$

where α_w and α_g are volume fraction of water and glycerin, and can be determined by solving a continuity equation for one (or more) of the phases. For the *i*-th phase, this equation has the following form:

$$\frac{\partial \alpha_i}{\partial t} + \nabla \cdot (\alpha_i \cdot \mathbf{u}) = 0 \tag{11}$$

where α_i is α_g or α_w. For the present homogeneous multiphase system consisting of water and glycerin, the above equation is solved for the volume fraction of glycerin. For the primary phase, which is water in this study, the volume fraction equation is not solved because in each computational cell, the volume fractions of all phases sum to unity. The volume fraction of water can be obtained from the following correlation:

$$\alpha_g + \alpha_w = 1 \tag{12}$$

3. Computational Grid

Considering the unsteady nature of the flow, the whole stirred tank was simulated. The determination of the grid resolution is a critical issue for numerical simulation. In this work, the grids were prepared by the pre-processor Gambit 2.3 according to the guidelines of Spalart [39,40]. A non-uniformly distributed hybrid unstructured mesh consisting of about 500,000 nodes was used. Much attention has been taken to putting more cells in the regions of high gradient around the blades and discharge region, where about 220,000 nodes were employed. Along the impeller width, 25 nodes were assigned with the minimal grid length equals to 0.008D. A similar grid resolution (970,997 cells for a stirred tank with a diameter T= 0.3 m and Re=4.17×10^4) was employed by Zadghaffari et al. [41] in their LES study of the turbulent flow and mixing in a stirred tank driven by a Rushton turbine, and satisfactory results were obtained. The grid used used here is also finer than the locally refined grid (0.023D) used by Revstedt et al. [42], who reported a good LES prediction of the turbulent flow. This implies that the grid resolution used here is adequate to resolve the turbulent flow accurately.

4. Modeling Method

All the simulations were performed with the commercial ANSYS 13.0 code, using the FLUENT fluid dynamics package, on a DEll T7500 workstation with two hex-core Xeon X5650 (2.67 GHz) processors and 32 GB RAM in a parallel model. To ensure smooth and better convergence, initially the k–ε computation was performed until the steady state flow field was obtained. Subsequently, the result of the steady-state computation was used as the initial solution to carry out the unsteady DES computation. For modeling the impeller rotation, the multiple reference frame (MRF) method was used in the k–ε computation. Then we switched to the fully transient

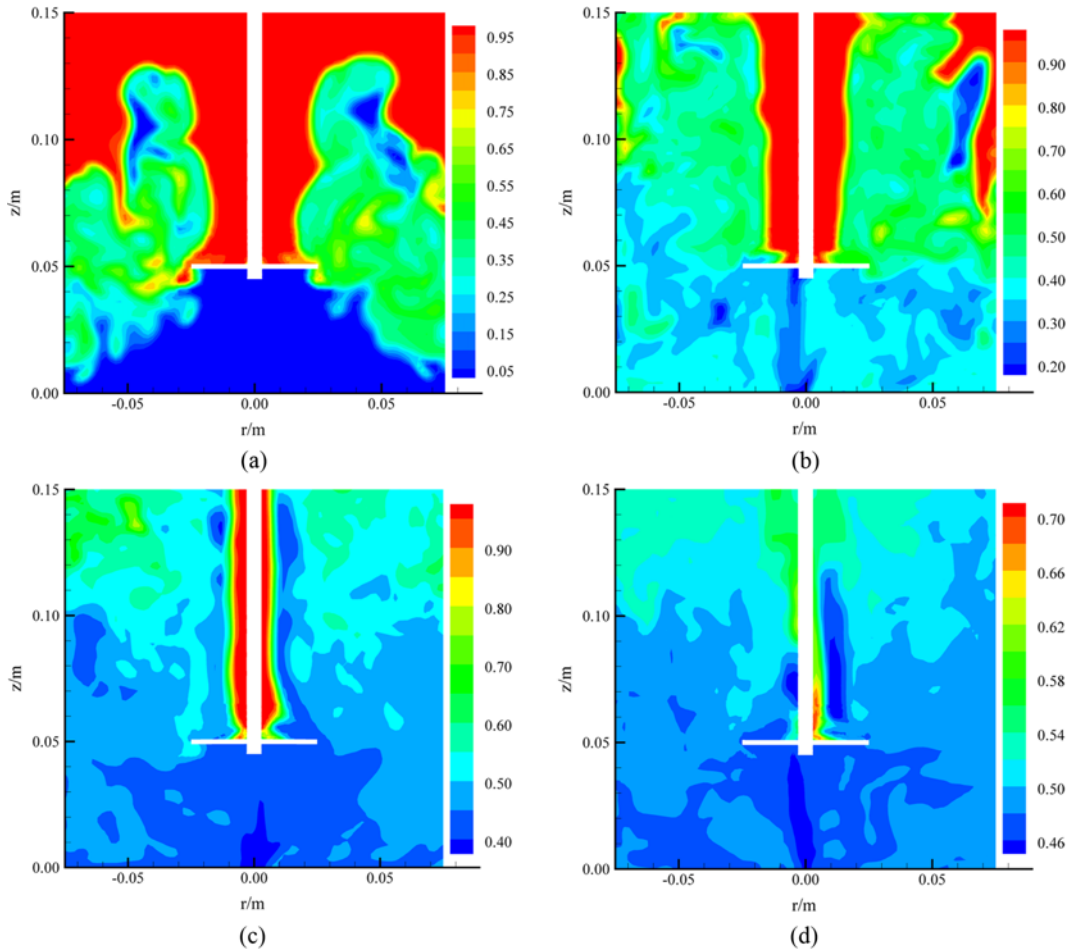

Fig. 2. Volume fraction of water in the cross section of the stirred tank at Ri=0.946: (a) 10, (b) 20, (c) 40 and (d) 60 impeller revolutions after startup.

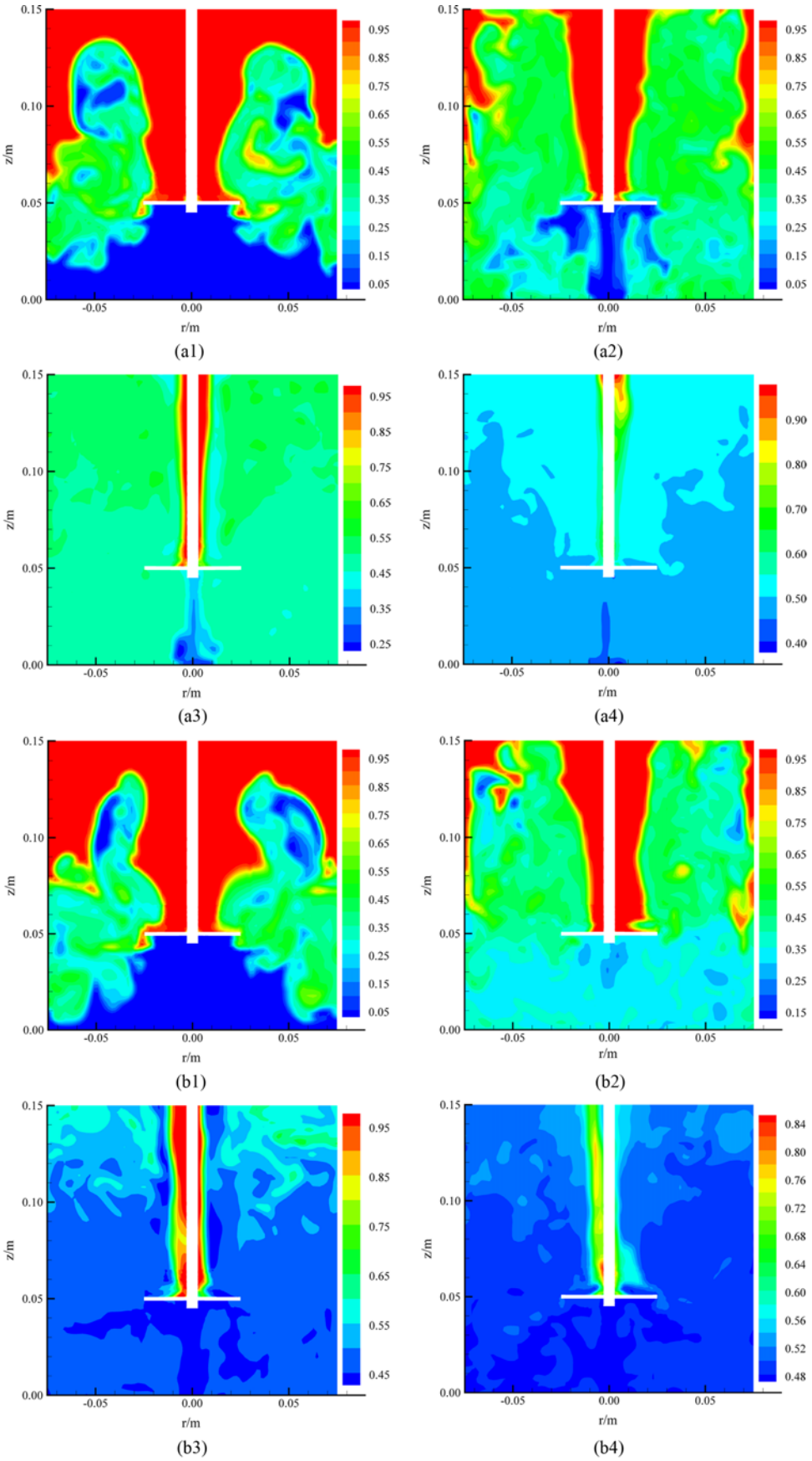

Fig. 3. Volume fraction of water in the cross section of the stirred tank at (a) Ri=0.236 and (b) Ri=1.478: (1) 10, (2) 20, (3) 40 and (4) 60 impeller revolutions after startup.

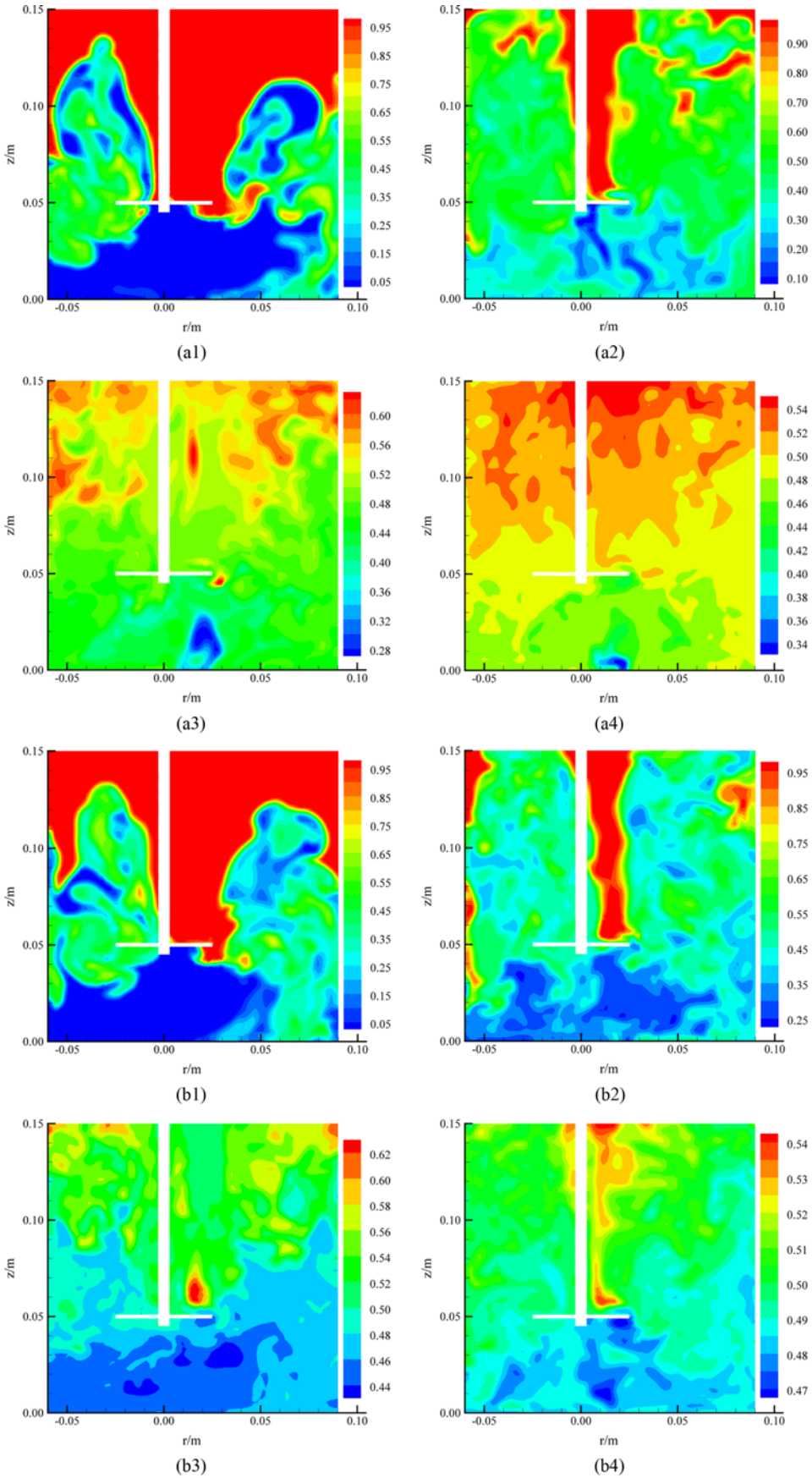

Fig. 4. Volume fraction of water in the cross section of the eccentrically stirred tank with e=0.2: (1) 10, (2) 20, (3) 40 and (4) 60 impeller revolutions after startup. From top to bottom, Ri=(a) 0.236, (b) 0.946 and (c) 1.478.

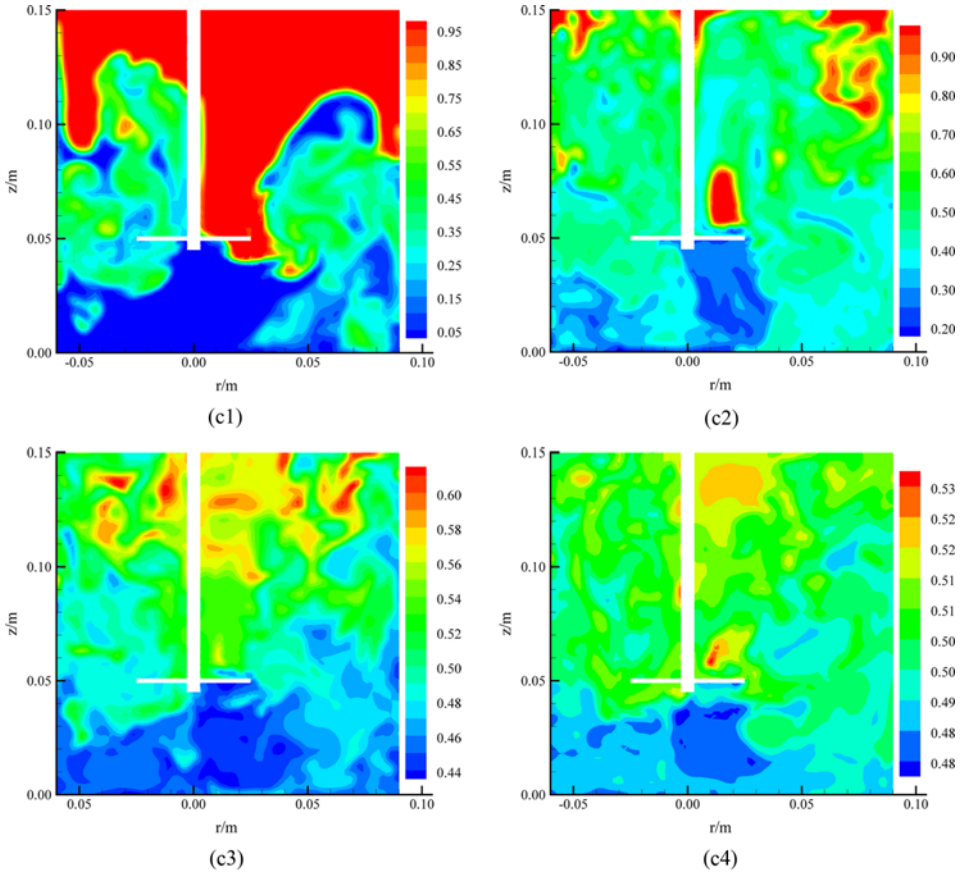

Fig. 4. Continued.

sliding mesh (SM) method for the DES computation. In this method, the rotation of the impeller is explicitly taken into account and two fluid zones are defined: an inner rotating cylindrical volume centered on the impeller (rotor region) and an outer stationary zone containing the rest of the tank (stator region). In our simulation, the boundary of the rotor region was positioned at r=0.075 m and 0.03 m<z< 0.07 m (where z is the axial distance from the bottom of the tank).

The initial condition for each simulation was that of still liquid. A flat liquid surface was assumed at the liquid surface. No-slip boundary conditions were used at the impeller blades, the shaft and the tank walls. For the steady-state k–ε simulation, the standard wall function was used to solve the near-wall flow. The SIMPLE algorithm was performed to couple velocities and pressure terms. The continuity equation, momentum conservation equation and k–ε equation were all discretized using the second order upwind scheme to obtain a high-precision result. For the DES computation, the PISO discretization scheme was adopted to couple velocities and pressure terms. Since second-order time discretization is not available with explicit VOF, the first-order implicit scheme was used for time discretization. An explicit VOF scheme with the implicit body force formulation was selected with the modified high resolution interface capturing (Modified HRIC) scheme to capture the interface. The modified HRIC scheme overcomes the deficiencies with the diffusive nature of upwind schemes and the unphysical results of central differencing schemes. This provides improved accuracy when compared to QUICK and second-order schemes, and is generally less computationally expensive than the Geo-Reconstruct scheme. The body force weighted scheme was employed to compute the pressure. The bounded central differencing scheme was utilized for spatial discretization of momentum and the modified turbulent viscosity equation. This scheme blends the pure central differencing

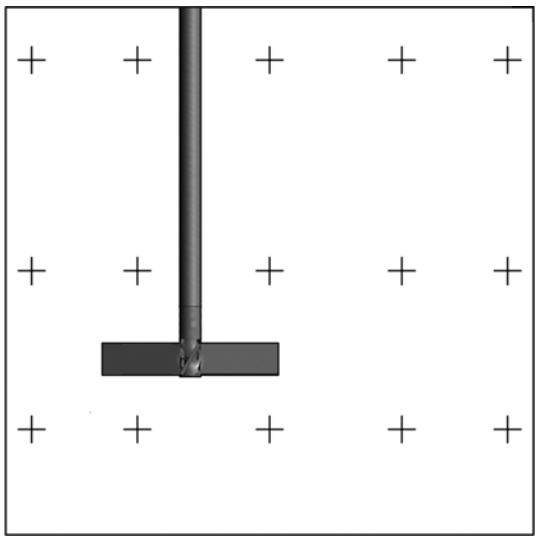

Fig. 5. Arrangements of the monitoring points (+) in the vertical middle plane of the stirred tank. From left to right, radial coordinates of the monitoring points are x*=−0.9, −0.5, 0, 0.5, 0.9. From top to bottom, axial coordinates of the monitoring points are z*=0.9, 0.5, 0.2.

scheme with first- and second-order upwind schemes, and can reduce the unphysical oscillations in the solution field induced by the central differencing scheme. For the VOF multiphase model, water was set as the primary phase and glycerin was set as the secondary phase. No effect of surface tension was considered.

The time step and number of iterations are crucial to transient DES modeling. The time step must be small enough to capture the flow features induced by the motion of the impeller. Furthermore, it also must be considered with the grid to ensure a stable and converged solution, especially when the VOF method is used. A variable time stepping method was used here, and an initial time step of $\Delta t=1\times10^{-5}$ s was adopted. The global courant number was set at no more than 2. Within each time step, a maximum of 20 iterations were performed and the solution was considered to be fully converged when the normalized residuals of all variables were less than 1×10^{-4}.

RESULTS AND DISCUSSION

1. Images of Concentration Fields

The results of our simulations will be mostly discussed in terms of the spatial and temporal evolutions of the volume fractions of water and/or glycerin under different operating conditions. The concentration fields from a still, stratified state across the cross-section of the stirred tank are mainly presented. As an illustration, the contours of volume fractions of water at Ri=0.946 at four different moments are given in Fig. 2.

It is apparent that each plot is almost symmetric about the axis

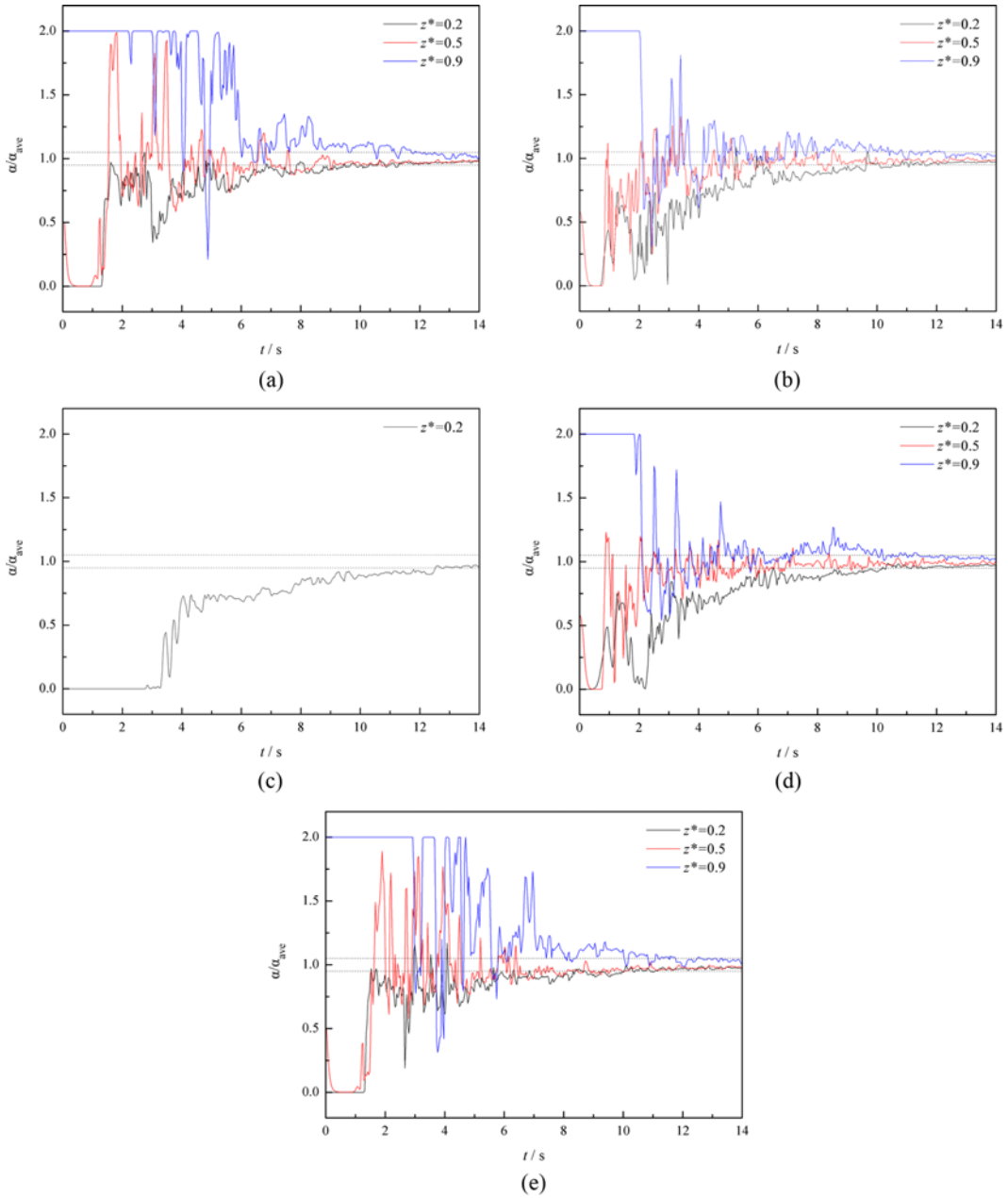

Fig. 6. Time variations of the volume fraction of water at radial positions x*=(a) −0.9, (b) −0.5, (c) 0, (d) 0.5, (e) 0.9. All cases: e=0, Ri=0.946.

of the stirred tank. After startup of the impeller, the fluids are first discharged toward the tank wall, and simultaneously, the integrity of the interface between water and glycerin in the impeller discharge flow region is quickly broken up. However, in the regions above and below the impeller, the interface stays horizontal and still maintains its integrity even after 10 impeller revolutions. Then because of the effect of the transient flow fields, glycerin appears in the upper parts of the stirred tank, water is pulled down to the lower region originally occupied by glycerin and is mixed with it. After about 20 impeller revolutions, the interface between the two miscible fluids in the regions above and below the impeller disintegrates. But the mixing is still not uniform at this moment. In the cross section of the stirred tank, the largest concentration difference exists in the vicinity of the axis and the region right underneath the impeller, largely because of poor mixing in these regions. Subsequently, the concentration difference is reduced to a limited range and a homogeneous mixing state is gradually approached.

2. Effect of Ri

The effect of Ri on the stratification of water and glycerin is discussed in this section. Here we presented the volume fraction contours of water at Ri=0.236 and Ri=1.478. These plots have their Ri=0.946 counterparts displayed in Fig. 2. The mixing patterns at the three different Ri numbers studied here are similar. However, as can be assessed from Fig. 3, buoyancy has an apparent influence on the mixing process. For the lower Ri=0.236, there is a faster variation of the interface. The concentration of the fluid in the cross section of the stirred tank is more uniform and, accordingly, the mixing process can be accelerated. However, for larger Ri, the mixing

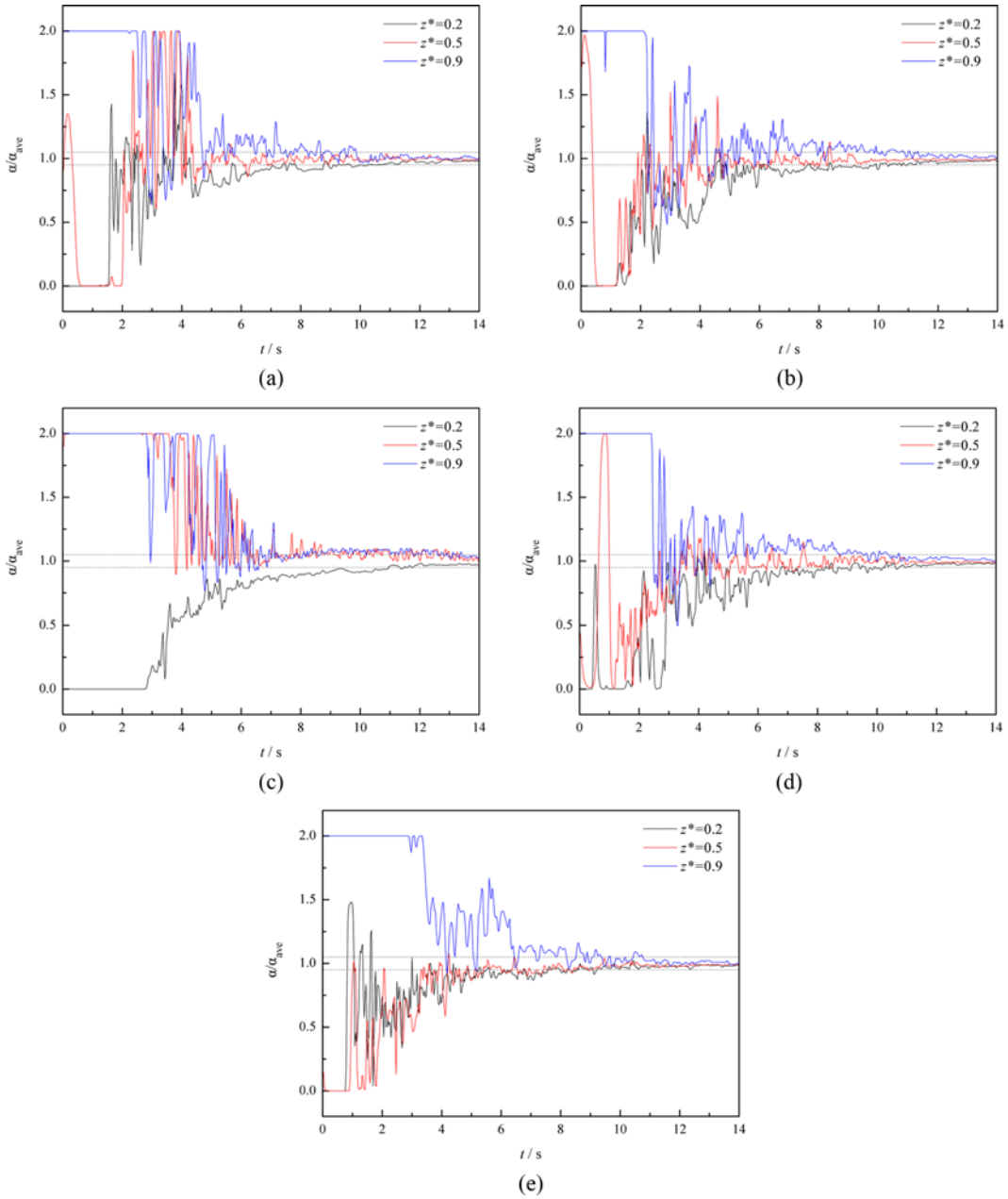

Fig. 7. Time variations of the volume fraction of water at radial positions x*=(a) −0.9, (b) −0.5, (c) 0, (d) 0.5, (e) 0.9. All cases: e=0.2, Ri=0.946.

process is hindered. This indicates that the presence of an interface acts as a barrier for the fluids mixing, which blocks the momentum transfer between the lighter and denser fluids, i.e., water and glycerin.

3. Effect of Eccentricity

The mixing performance of a stirred tank with no baffle is usually not perfect because of the lower axial circulation flow capacity. Accordingly, eccentric agitation was proposed by several authors. A better performance can be obtained by this agitation scheme, which perturbs the flow fields through breaking the spatial symmetry of the stirred tank and induces a chaotic mixing state. It has been identified that both the mixing performance and power consumption of eccentric agitation increase with the eccentricity. A compromise can be made when the eccentricity is about e=0.2. The stratified mixing processes of water and glycerin under this eccentricity are investigated here. Fig. 4 shows the volume fractions of water and glycerin in the cross section of the stirred tank in this case.

As can be seen from these plots, the spatial and temporal evolution of concentration fields of the two miscible fluids under eccentric agitation configuration are somewhat like their counterparts listed in Fig. 2 and 3: After startup, it takes about 20 impeller revolutions for the action of the impeller to be felt throughout the tank with the top of the stirred tank, and at this moment, in the vicinity of the stirred tank axis, there still exists a rather quiescent flow region where agitation is largely attributed to the rotation of the shaft, and not so much the result of the impeller. But essentially, there are significant differences between the mixing patterns of concentric and eccentric agitation. For the latter, the symmetry of the mixing patterns at different Richardson numbers is broken up. In addition, the effect of Ri on the mixing process is different. For higher Ri (0.946 and 1.478), a faster mixing process can be achieved when compared with that of concentric agitation configuration. By comparison, for, Ri=0.236 an opposite effect can be observed. This will be quantificationally analyzed in the following section.

4. Quantitative Analysis of Mixing Time

The mixing process can be quantificationally evaluated by mixing time. For the mixing of miscible fluids which involves introducing the scalar tracer into the bulk fluid, the t_{95} mixing time is traditionally used, which is defined as the time required from a non-equilibrium condition to achieve within a value of ±5% of the final concentration. Analogously, mixing time of the stratified miscible fluids studied here was computed based on the time evolutions of the volume fractions of water and glycerin. It is defined as the time required for the volume fraction to approach within ±5% of the average value. The mixing process is usually not uniform, and a total of 15 monitoring points in the vertical middle plane of the stirred tank were selected, and the volume fraction evolutions of water and glycerin with the time were examined. The arrangements of monitoring points are given in Fig. 5 and their axial and radial positions were ($z^*=z/T=0.2, 0.5, 0.9$) and ($x^*=2x'/T=\pm0.9, \pm0.5$m 0, where $x'=x-E$), respectively.

The numerically determined evolutions of the volume fraction of water at the selected monitoring positions for the cases e=0, Ri=0.946 and e=0.2, Ri=0.946 are shown in Fig. 6 and 7, respectively. In these plots, the volume fractions were made dimensionless by dividing the final averaged value. For the case of e=0, the two positions of $z^*=0.5$ and 0.9 are occupied by the shaft of the stirred tank and, accordingly, no data for mixing time is available at these two points. For other positions, there are large fluctuations in the initial stages of the mixing processes. Then there is a rapid change and it approaches the averaged value asymptotically. For other cases, similar time evolution trend of the scalar tracer concentration can be obtained. For the reason of simplicity, these plots are not given here.

From the plots of time variations of the scalar concentration, the t_{95} mixing time for the concentric and eccentric agitations can be obtained and the results are listed in Table 1. From this table, we can find the relationship between mixing time and Ri: the higher

Table 1. Numerically predicted mixing times for the stratified miscible fluids in the concentric (e=0) and eccentric (e=0.2) stirred tanks

Monitoring points (x^*, z^*)	Mixing time, t_{95}/s					
	e=0			e=0.2		
	Ri=0.236	Ri=0.946	Ri=1.478	Ri=0.236	Ri=0.946	Ri=1.478
(−0.9, 0.2)	4.97	11.29	13.84	6.00	10.75	13.36
(−0.9, 0.5)	4.61	10.87	12.34	5.05	7.04	9.01
(−0.9, 0.9)	4.97	11.86	14.54	5.35	9.88	13.12
(−0.5, 0.2)	4.61	11.79	13.63	6.68	10.98	13.32
(−0.5, 0.5)	4.32	8.56	11.82	4.08	8.40	11.64
(−0.5, 0.9)	4.79	12.12	14.31	6.89	11.34	13.57
(0, 0.2)	8.23	12.82	15.11	7.09	11.79	13.97
(0, 0.5)	\	\	\	7.22	13.29	13.64
(0, 0.9)	\	\	\	9.01	13.41	13.43
(0.5, 0.2)	4.68	11.65	13.67	7.22	10.98	13.61
(0.5, 0.5)	3.89	9.53	12.63	3.93	8.77	10.07
(0.5, 0.9)	4.61	11.39	13.39	6.45	10.75	12.81
(0.9, 0.2)	4.90	11.19	13.35	5.21	9.24	13.26
(0.9, 0.5)	4.11	10.03	13.27	4.97	8.96	10.25
(0.9, 0.9)	4.75	12.59	13.71	5.95	10.78	12.60
t_{ave}	4.88	11.21	13.51	6.07	10.42	13.18

Ri, the larger the mixing time. As described in section 2, the two miscible fluids have fixed properties, and Ri and Re are altered by adjusting the impeller rotation speed N. Besides, Re is proportional to N, and Ri decrease with increasing N. Consequently, we can also say that the larger Ri, the lower the mixing time. This is in accordance with the results of Derksen [19,20]. Table 1 also shows how the mixing time relates to eccentricity e. For higher Ri, the mixing time obtained when e=0.2 is slightly lower than that of e=0. For example, the differences are within 7% for Ri=0.946. When Ri=1.478, the differences are reduced to less than 2%. However, the situation is reversed for lower Ri. The average mixing time is 24.4% longer than the mixing time obtained with the concentric agitation when Ri=0.236. This finding indicates that eccentric agitation is not suitable for the low-viscosity stratified miscible fluids mixing, especially when Ri is not so large. The drawback of eccentric agitation has also been identified by Ascanio et al. [43]. They found that the role that impeller position plays is highly dependent on the fluid viscosity. In some cases, an impeller off-centered position with low viscosity fluids can lead to longer mixing times, especially when axial flow impellers, such as the pitched-blade turbine, are used.

From Table 1, we can also see that mixing time is a local variable, which depends on the position of the monitoring point. For eccentric agitation (e=0.2), the differences in mixing times among different positions are large and changing Ri can mitigate this effect: the lower Ri, the larger difference. At Ri=1.478, the mixing time differences are within 55%. When Ri=0.946, this has grown to some 90%. By Ri=0.236, the maximum difference is as high as about 129%. By contrast, the variations in the mixing times for e=0 are not so much: from Ri=1.478, 0.946 to 0.236, the maximum mixing time difference is 28%, 50% and 110%. This result shows that eccentric agitation cannot improve the uniformity for the low-viscosity stratified miscible fluids mixing, even though it can somewhat reduce the averaged mixing time for higher Ri.

CONCLUSIONS

A combination of DES model and VOF technique was used to study the mixing of two initially stratified miscible fluids, i.e., water and glycerin, with different density and viscosity in this study. The impeller was considered with the details of the blade geometry and the sliding mesh method was used to predict the impeller rotation. The mixing processes and mixing times were simulated using the commercial CFD software Fluent 13.0. The effects of Richardson number Ri and impeller eccentricity e on the mixing time were quantificationally analyzed. It was found that mixing time increases with increasing Ri. For higher Ri, the mixing time can be slightly reduced by eccentric agitation. But for lower Ri, the situation is even reversed. In addition, eccentric agitation cannot improve mixing uniformity. Therefore, it is unadvisable to use the eccentric agitation scheme to blend the low-viscosity miscible fluids starting from a stratified state.

Finally, although the studies performed here are purely computational, the results are amenable to experimental verification. Some techniques, such as planar laser induced fluorescence (PLIF) and electrical resistance tomography (ERT), can be employed to visualize the mixing process. In this sense, another aim of this paper is to evoke experimental investigation of the flow systems similar to the one studied here. Because of the stirred tank layout, the initial conditions of the fluids to be mixed and their properties have significant consequences for the mixing process. Another demerit of this contribution is that only one eccentricity and three Richardson numbers are covered. Other than Richardson number and eccentricity, mixing time also depends on the geometry of the mixing device (impeller and tank layout), the operating conditions (such as impeller speed), and the liquids involved in the mixing process. More works should the carried out so as to establish an equation that correlates all the parameters to the mixing time.

ACKNOWLEDGEMENT

Support from NSFC (Natural Science Foundation of China) (No. 21306105) is gratefully acknowledged.

REFERENCES

1. R. Shinnar, *J. Fluid Mech.*, **10**, 259 (1961).
2. N. Harnby, M. F. Edwards and A. W. Nienow, *Mixing in the process industries*, Butterworth-Heinemann, Oxford, 2nd Ed. (1997).
3. B. J. Briscoe, C. J. Lawrence and W. G. P. Mietus, *Adv. Colloid Interface Sci.*, **81**, 1 (1999).
4. H. Yapici and G. Basturk, *Comput. Chem. Eng.*, **28**, 2233 (2004).
5. T. Lemenand, P. Dupont, D. Della Valle and H. Peerhossaini, *J. Fluids Eng.*, **127**, 1132 (2005).
6. T. Lemenand, C. Durandal, D. Della Valle and H. Peerhossaini, *Int. J. Therm. Sci.*, **49**, 1886 (2010).
7. J. J. Derksen and H. E. A. Van Den Akker, *Chem. Eng. Res. Des.*, **85**, 697 (2007).
8. R. K. Grenvilie and A. W. Nienow, In: *Handbook of Industrial Mixing: Science and Practice*, E. L. Paul, V. A. Atiemo-Obeng and S. M. Kresta Eds., John Wiley & Sons Inc., Hoboken, NJ (2004).
9. J. M. Smith and A. W. Schoenmakers, *Chem. Eng. Res. Des.*, **66**, 16 (1988).
10. I. Bouwmans and H. E. A. Van den Akker, *IChemE Symp. Ser.*, **121**, 1 (1990).
11. I. Bouwmans, A. Bakker and H. E. A. van den Akker, *Chem. Eng. Res. Des.*, **75**, 777 (1997).
12. P. R. Gogate and A. B. Pandit, *Can. J. Chem. Eng.*, **77**, 988 (1999).
13. R. Mann, M. Wang, A. E. Forrest, P. J. Holden, F. J. Dickin, T. Dyakowski and R. B. Edwards, *Chem. Eng. Commun.*, **175**, 39 (1999).
14. S. Kim, A. N. Nkaya and T. Dyakowski, *Int. Commun. Heat Mass Transfer*, **33**, 1088 (2006).
15. G. Madras and B. J. McCoy, *J. Fluids Eng.*, **127**, 564 (2005).
16. Y. Jang and S. M. de Bruyn Kops, *Comput. Fluids*, **36**, 238 (2007).
17. J. G. van de Vusse, *Chem. Eng. Sci.*, **4**, 178 (1955).
18. C. D. Rielly and A. B. Pandit, *Proceedings of 6th European conference on mixing*, Pavia, **69** (1988).
19. J. J. Derksen, *Comput. Fluids*, **50**, 35 (2011).
20. J. J. Derksen, *Ind. Eng. Chem. Res.*, **51**, 6948 (2012).
21. H. J. S. Fernando, *Annu. Rev. Fluid Mech.*, **23**, 455 (1991).
22. J. M. Holford and P. F. Linden, *Dyn. Atmos. Oceans*, **30**, 173 (1999).
23. G. N. Ivey, K. B. Winters and J. R. Koseff, *Annu. Rev. Fluid Mech.*, **40**, 169 (2008).
24. P. Müller and C. Garrett, *J. Oceanogr.*, **15**, 12 (2002).
25. S. Remmler and S. Hickel, *Int. J. Heat Fluid Flow*, **35**, 13 (2012).
26. F. L. Yang, S. J. Zhou and G. C. Wang, *Comput. Fluids*, **64**, 74

(2012).
27. A. Serra, M. Campolo and A. Soldati, *Chem. Eng. Sci.*, **56**, 2715 (2001).
28. J. N. Haque, T. Mahmud and K. J. Roberts, *Ind. Eng. Chem. Res.*, **45**, 2881 (2006).
29. G. M. Cartland Glover and J. J. Fitzpatrick, *Chem. Eng. J.*, **127**, 11 (2007).
30. J.-P. Torré, D. F. Fletcherb, T. Lasuyec and C. Xuereb, *Chem. Eng. Sci.*, **62**, 6246 (2007).
31. T. Mahmud, J. N. Haque, K. J. Roberts, D. Rhodes and D. Wilkinson, *Chem. Eng. Sci.*, **64**, 4197 (2009).
32. N. Lamarque, B. Zoppé, O. Lebaigue, Y. Dolias, M. Bertrand and F. Ducros, *Chem. Eng. Sci.*, **65**, 4307 (2010).
33. M. Jahoda, M. Moštěk, I. Fořt and P. Hasal, *Can. J. Chem. Eng.*, **89**, 717 (2011).
34. J. Gimbun, C. D. Rielly, Z. K. Nagy and J. J. Derksen, *AIChE J.*, **58**, 3224 (2012).
35. F. L. Yang, S. J. Zhou, C. X. Zhang, G. M. Evans and G. C. Wang, *Chem. Eng. Commun.*, **200**, 1347 (2013).
36. M. Strelets, AIAA-2001-0879.
37. X. X. Li and Y. X. Ren, *J. Tsinghua Univ. (Sci. & Technol.)*, **44**, 1126 (2004).
38. P. R. Spalart, W. H. Jou, M. Strelets and S. R. Allmaras, In: *Advances in DNS/LES* C. Liu and Z. Liu Eds., Greyden Press, Columbus, OH (1997).
39. P. R. Spalart, NASA/CR-2001-211032.
40. P. R. Spalart, *Annu. Rev. Fluid. Mech.*, **41**, 181 (2009).
41. R. Zadghaffari, J. S. Moghaddas and J. Revstedt, *Comput. Fluids*, **39**, 1183 (2010).
42. J. Revstedt, L. Fuchs and C. Trägårdh, *Chem. Eng. Sci.*, **53**, 4041 (1998).
43. G. Ascanio, M. Brito-Bazán, E. Brito-De La Fuente, J. Pierre, P. J. Carreau and P. A. Tanguy, *Can. J. Chem. Eng.*, **80**, 558 (2002).